Improving power conversion efficiency of perovskite solar cells by cooperative LSPR of gold-silver dual nanoparticles*

Peng Liu(刘鹏)[1], Bing-chu Yang(杨兵初)[1,†], Gang Liu(刘钢)[1], Run-sheng Wu(吴闰生)[1,3], Chu-jun Zhang(张楚俊)[1], Fang Wan(万方)[1], Shui-gen Li(李水根)[1,3], Jun-liang Yang(阳军亮)[1], Yong-li Gao(高永立)[1,2], and Cong-hua Zhou(周聪华)[1,‡]

[1] *Hunan Key Laboratory of Super Microstructure and Ultrafast Process, School of Physics and Electronics, Central South University, Changsha* 410083, *China*
[2] *Department of Physics and Astronomy, University of Rochester, Rochester, New York* 14627, *USA*
[3] *School of New Energy Science and Engineering, Xinyu University, Xinyu* 338004, *China*

(Received 8 January 2017; revised manuscript received 17 February 2017; published online 6 April 2017)

Enhancing optical and electrical performances is effective in improving power conversion efficiency of photovoltaic devices. Here, gold and silver dual nanoparticles were imported and embedded in the hole transport layer of perovskite solar cells. Due to the cooperative localized surface plasmon resonance of these two kinds of metal nanostructures, light harvest of perovskite material layer and the electrical performance of device were improved, which finally upgraded short circuit current density by 10.0%, and helped to increase power conversion efficiency from 10.4% to 11.6% under AM 1.5G illumination with intensity of 100 mW/cm^2. In addition, we explored the influence of silver and gold nanoparticles on charge carrier generation, dissociation, recombination, and transportation inside perovskite solar cells.

Keywords: light harvest, perovskite solar cells, silver nanoparticle, gold nanoparticle

PACS: 84.60.Jt, 88.40.H–, 73.20.Mf, 78.67.–n **DOI:** 10.1088/1674-1056/26/5/058401

1. Introduction

Organic-inorganic perovskite ($CH_3NH_3PbX_3$, X = Cl, Br and I or the mixture) solar cells (PSCs) have attracted ever-increasing attention over the last few years due to excellent photovoltaic response, ease of fabrication, and low-cost precursor materials.[1–3] In particular, power conversion efficiencies (PCE) of PSCs have been upgraded from 3.8% to higher than 20% in the past seven years,[4–6] rendering them competitive candidates of commercial crystalline silicon solar cells.

In order to improve photo-to-electric energy conversion efficiency, many strategies have been developed, such as interface modification engineering,[7,8] morphology optimization,[9–11] and device structure designing.[12,13] These measures mainly focus on improving the electrical properties of the PSCs to minimize the charge carrier loss to achieve a high PCE. However, the performance of PSCs is still limited by insufficient light absorption.[14–16] Therefore, increasing light harvest is also a useful method to upgrade efficiency of photovoltaic cells. For thin film based solar cells, increasing film thickness is effective for light harvest, but it usually suffers from the increased recombination rate due to longer transporting distance of photo-generated charge carrier.[10,17] As a result, it is necessary to keep balance between the electrical and optical benefits of the cells. Therefore, enhancing light absorption while avoiding increase of thickness of active layer is preferred.

Metallic nanoparticles (NPs) have been found to improve the light harvest of solar cells due to localized surface plasmon resonance (LSPR),[18] and have been utilized in a variety of solar cells including dye-sensitized solar cells,[19,20] organic solar cells,[2,21,23] and recently, were also introduced into PSCs.[15,16,24] However, with this approach, the metallic NPs incorporated into the perovskite layer could cause interface problem which sacrifice PSCs electrical properties, as well as increase the complexity of fabricate of device. Usually, they used only one kind of NPs, but it is plasmonic effect just aroused from single resonance enhancement of nanoparticle. Different metallic NPs can be embedded into hole transport layer (HTL), which induce different resonance enhancement of different nanoparticles without sacrificing PSCs electrical properties and increasing the complexity of fabricate of device, such as Au and Ag NPs.[25] In addition, the influence of NPs on charge carrier separation and transport inside high efficiency PSCs still needs to be explored in depth.

Here we induced dual metallic nanoparticles (dual NPs), Au and Ag NPs, into the HTL of PSCs. This simple approach helps to increase the average PCE from 10.4% to 11.6% under one sun in AM 1.5G, attributed to the improvement in photocurrent. Moreover, we revealed the role of dual NPs on photocurrent generation of PSCs, using various means of ultraviolet–visible spectrophotometer, external quantum effi-

*Project supported by the National Natural Science Foundation of China (Grant Nos. 61306080, 51203192, 11334014, and 51664047), the Natural Science Foundation of Hunan Province, China (Grant No. 2015JJ3143), and the Scientific and Technological Project of Hunan Provincial Development and Reform Commission, China.

†Corresponding author. E-mail: bingchuyang@csu.edu.cn
‡Corresponding author. E-mail: chzhou@csu.edu.cn

© 2017 Chinese Physical Society and IOP Publishing Ltd

ciency, and electrochemical impedance spectroscopy spectra.

2. Experiments and characterizations

PSCs without and with dual NPs were fabricated in structure of ITO/PEDOT:PSS/$CH_3NH_3PbI_3$/PCBM/Al, as shown in Fig. 1. A typical cross-sectional scanning electron microscope image of the perovskite device is demonstrated in Fig. A1 of Appendix A. Typically, PEDOT:PSS (PVP AI 4083, Baytron) layer without and with dual NPs were spin-coated on clean ITO substrate with a speed of 3000 rpm and annealed on hot plate at 150 °C for 15 min. To incorporate dual NPs, solution of dual NPs (0.01% in DI water, Beijing DK nano technology Co-LTD) was mixed with PEDOT:PSS solution with volume ratio of 1:6. Then the active layer of perovskite material was deposited on the top of the above film by spin-coating and annealed at 100 °C for 10 min in glove box with high N_2 gas background (both H_2O and $O_2 < 1.0$ ppm). In order to obtain high-quality perovskite film, the solvent induced fast crystallization deposition (SIFCD) method was used.[26–28] The perovskite layer was then covered by a thin layer of fullerene derivative PCBM (Dye Source, USA). Finally, alumina electrode (100 nm ca. in thickness) was deposited by thermal evaporation under vacuum of $\sim 4\times10^{-6}$ mbar, after which the entire PSCs with active area of 0.0906($\pm$0.0009) cm^2 was completed.

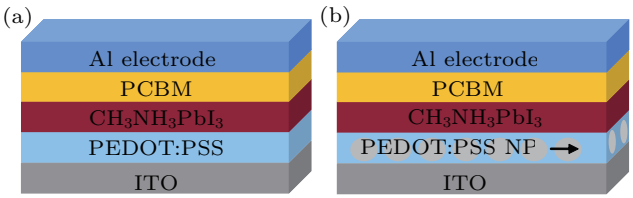


Fig. 1. (color online) Schematic of device structure of PSCs (a) without NPs and (b) with gold-silver dual NPs.

The absorption spectra of $CH_3NH_3PbI_3$ films and NPs dispersed in deionized water were measured by ultraviolet–visible spectrophotometer (UV–vis, Puxi, T9, China). Surface enhanced Raman scattering (SERS) was measured by laser-Raman microspec-troscopy (LabRAM HR800). Morphological properties of these metal nanoparticles as well as the perovskite films were monitored by transmission electron microscopy (TEM, JEM-2100F, Japan), scanning electron microscopy (FEI Helios Nanolab 600i SEM, USA), and atomic force microscopy (AFM, Agilent Technologies, model 5500, USA), respectively. Current density versus voltage (J–V) characteristics of the devices were tested by digital source meter (Keithley, model 2420, USA) together with a solar simulator (91160s, Newport, AM 1.5G, 100 mW/cm^2). The external quantum efficiency (EQE) was performed by a spectrum performance testing system (7-SCSpec, Saifan, China). The steady state photoluminescence (PL) spectra were recorded by fluorescence spectrophotometer (F-2500, HITACHI, Japan) under air ambient conditions. Electrochemical impedance spectroscopy (EIS) of the solar cells was performed by electrochemical work station (CHI660D, Chenhua, China) under 1 sun AM 1.5G illumination.

3. Results and discussion

Figure 2(a) shows TEM image of dual NPs. TEM images of single Au and Ag NPs are showed in Fig. A2 of Appendix A. These dual NPs are around 50 nm in diameter, which are comparable to the thickness of the PEDOT:PSS layer. Therefore, dual NPs are appropriately embedded in PEDOT:PSS layer and LSPR is induced by dual NPs near the active layer of our devices.[25] The absorption spectrum of dual NPs dispersed in deionized water monitored by UV–vis is displayed in Fig. 2(b). Two absorption peaks at around 410 and 525 nm could be distinguished, which is attributed to LSPR of Ag and Au NPs, respectively. It is the dual resonant peaks of dual NPs that exhibits photovoltaic devices with dual NPs own better improvement on the performance than that of single NPs.[25] The absorption spectra of single Au and Ag NPs are shown in Fig. A3 of Appendix A, and both of them have only one absorption peak.

To better illustrate the enhancement of local electrical field induced by LSPR, SERS measurements were performed using Rhodamine 6G (R6G) as the probe molecule and dual NPs loaded ITO glass as SERS substrate. Electrical field enhancement is a major effect commonly considered as the origin of the enhanced Raman signal and it is a consequence of the interaction of the incoming laser radiation with electrons in the metal surface, which activates LSPR of the metal electrons.[29] Before testing, R6G solution (10^{-3} mol/L in concentration) was dropped on. For comparison, bare ITO glass was also examined and the Raman signal is shown in Fig. 2(d). As shown in Fig. 2(c), the intensity is increased by 200 times for dual NPs loaded SERS substrate, thus clearly showing that electric field near the NPs has been enhanced by the LSPR.

In order to further confirm that NPs are imbedded within PEDOT layer, the AFM topography images of PEDOT:PSS without and with dual NPs are shown in Figs. 3(a) and 3(b), respectively. The root-mean-squared (RMS) roughness of PEDOT:PSS layer on ITO glass is measured to be 1.52 nm, while PEDOT:PSS mixed with dual NPs exhibits almost the same RMS roughness which is 1.53 nm. Given the RMS roughness change slightly, the dual NPs are suggested to be buried within the PEDOT:PSS layer. Figures 3(c) and 3(d) exhibit the SEM of the surface morphology of $CH_3NH_3PbI_3$ thin films deposited on the PEDOT:PSS layer without and with dual NPs respectively. The two kinds of the surface morphology of perovskite thin films are similar, which is continuous and compact. These results suggest that incorporating dual NPs into the PEDOT:PSS neither increase the recombination center nor affect the growth of the active layer.

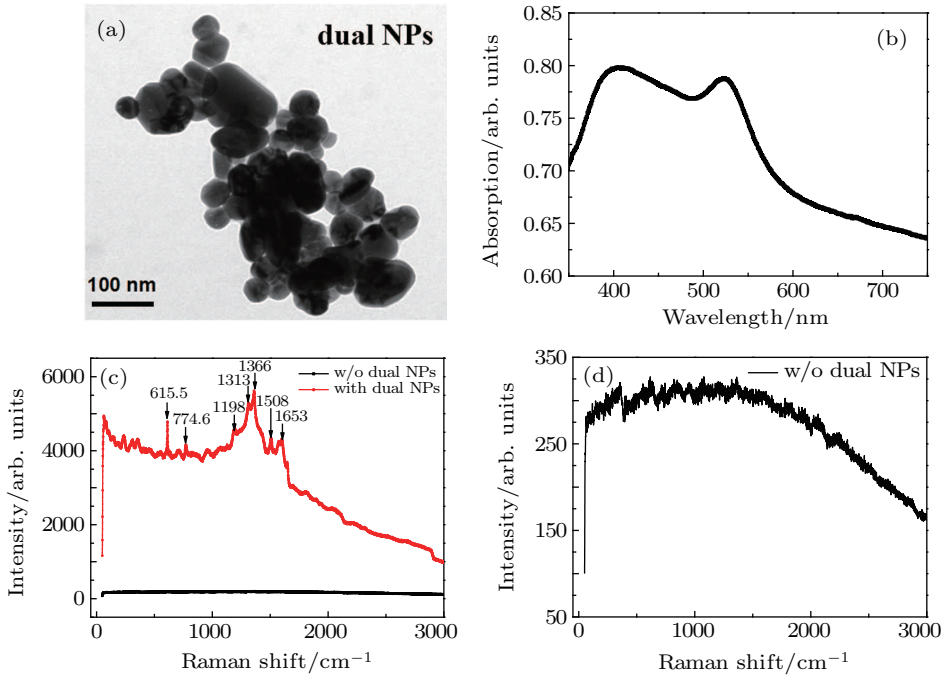


Fig. 2. (color online) (a) TEM image of dual NPs. (b) Absorption spectrum of dual NPs dispersed in deionized water. (c) Raman signal of 10^{-3} mol/L rhodamine on ITO glass without and with dual NPs. (d) Raman signal of 10^{-3} mol/L rhodamine on bare ITO glass.

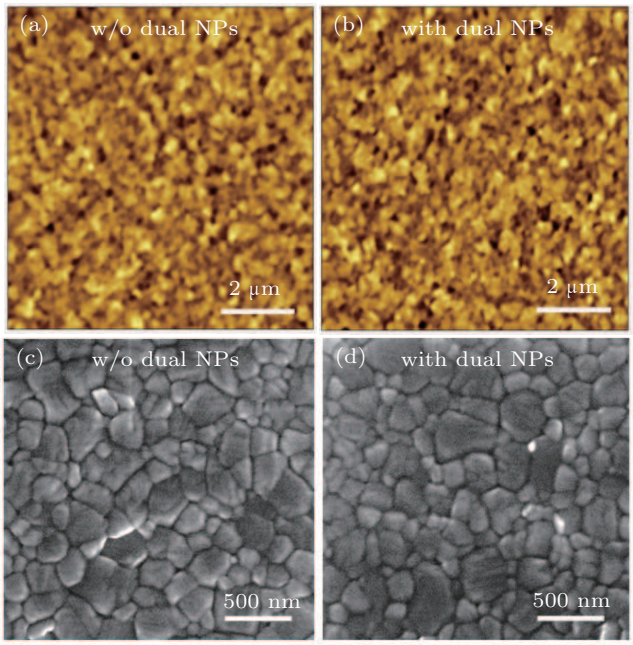


Fig. 3. (color online) AFM images of PEDOT:PSS (a) without and (b) with dual NPs. SEM images of perovskite thin films deposited on the PEDOT:PSS (c) without and (d) with dual NPs.

To clarify the effect of dual NPs in PSCs performance, the PSCs without and with dual NPs were fabricated and the PCE were measured. Typical J–V characteristics curves of PSCs without and with dual NPs are shown in Fig. 4(a). Addition of dual NPs help to increase J_{sc} from 18.26 to 21.07 mA/cm^2. To objectively evaluate the photovoltaic performance, more experiments were carried out. The statistic parameters of device performance under different scanning directions over 10 of each device without and with dual NPs are shown in Table 1. After incorporating dual NPs into PEDOT:PSS layer, open-circuit voltage (V_{oc}) and fill factor (FF) remain unchanged relatively, while J_{sc} increases from 18.59 to 20.45 mA/cm^2. As a result, the average PCE increases from 10.43% to 11.62%. In addition, the smaller standard deviations of devices with dual NPs indicate good reliability and reproducibility. Furthermore, the PSCs with dual NPs do not show obvious hysteresis when changing the scanning direction, as shown in Fig. 4(b). The PCE of 12.21% and 12.49% were obtained at the scanning direction from negative to positive bias and from positive to negative bias, respectively. These almost no hysteresis suggests that the device performance could be improved with the assistance of dual NPs.[5]

External quantum efficiency (EQE) of PSCs were conducted to explore the cause of improved J_{sc}. Figure 5(a) depicts the corresponding EQE spectra. For device with dual NPs, significant enhancement in EQE takes place over almost the whole absorption range of perovskite material. The integrated J_{sc} values calculated from our EQE spectrum for devices without and with dual NPs are 16.43 and 18.48 mA/cm^2, respectively. The small deviation between the integrated J_{sc} and that from J–V curves come from incomplete absorption of chromic light, and trap. To explore the effect of the LSPR on the charge carrier generation behavior, we performed steady state PL measurements. Figure 5(b) presents the room temperature PL spectra for the samples that were prepared by spin-coating perovskite films onto the PEDOT:PSS without and with the dual NPs. The integrating PL intensity of the sample with dual NPs is enhanced by ca. 12% with respect to that of the sample without dual NPs when we excited the sample at 380 nm. The enhancement of PL intensity is attributed to the

fact that excitation of the LSPR increased the degree of light absorption and the strong interactions between plasmonic field and excitons enhanced the light excitation rate.[30,31] To better illustrate the J_{sc} enhancement, the UV–vis absorption spectra of ITO/PEDOT:PSS without and with dual NPs /$CH3NH_3PbI_3$ films are measured as shown in Fig. 5(c). The absorption in the region of wavelengths from 350 to 500 nm is obviously enhanced after incorporating dual NPs. The enhanced absorption is in good agreement with the plasmonic resonance region of dual NPs (Fig. 2(b)). The UV–vis transmittance spectra of PEDOT:PSS without and with dual NPs are shown in Fig. 5(d). Compared with the PEDOT:PSS, the slight increase of UV–vis transmittance of PEDOT:PSS with dual NPs. On the basis of the UV–vis absorption in Fig. 5(c) and the UV–vis transmittance in Fig. 5(d), it is clear that the absorption enhancement in Fig. 5(c) mainly occur in perovskite films. These results indicate that PSCs with dual NPs show a plasmonic effect that is caused by the LSPR absorption.[15,16,25] However, this LSPR absorption cannot absolutely explain enhancement in J_{sc} of the PSCs. In Fig. 5(a), the enhancement in the EQE of the PSCs by the dual NPs is observed in the region of wavelengths from 350 to 750 nm rather than from 350 to 500 nm. This result suggests that there are other reasons for the increase in the J_{sc} of PSCs with dual NPs in addition to the LSPR absorption. The increase in EQE of device with dual NPs could be partially attributed to the improved electrical properties over a wide region of wavelength,[15,16,22,24,25,31,32] and will be discussed in detail in the following.

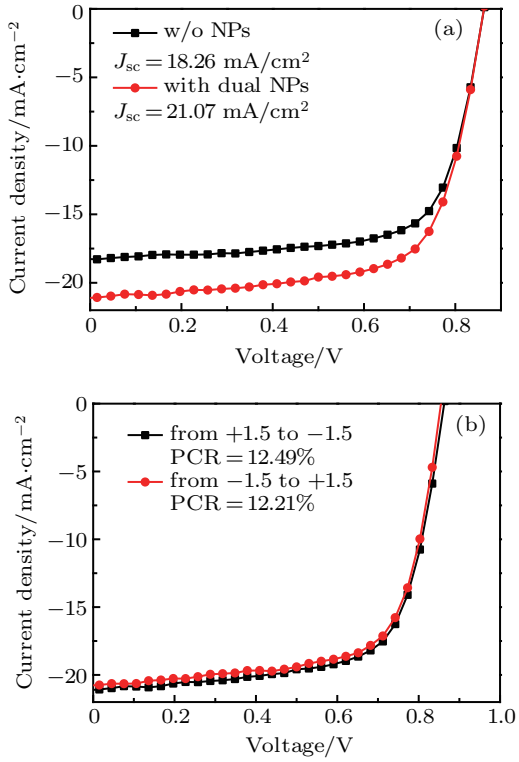


Fig. 4. (color online) (a) Typical *J*–*V* curves of PSCs without and with dual NPs. (b) *J*–*V* curves of the PSCs with dual NPs under different scanning directions at scanning speed of 0.3 V/s.

Table 1. Average photovoltaic parameters and standard deviations of PSCs without and with dual NPs under AM 1.5G illumination at 100 mW/cm^2.

Dual NPs	J_{sc}/mA·cm^{-2}	V_{oc}/V	FF/%	PCE/%
W/O	18.59±0.69	0.82±0.02	67.97±2.19	10.4±0.74
With	20.45±0.38	0.83±0.01	67.65±1.72	11.6±0.59

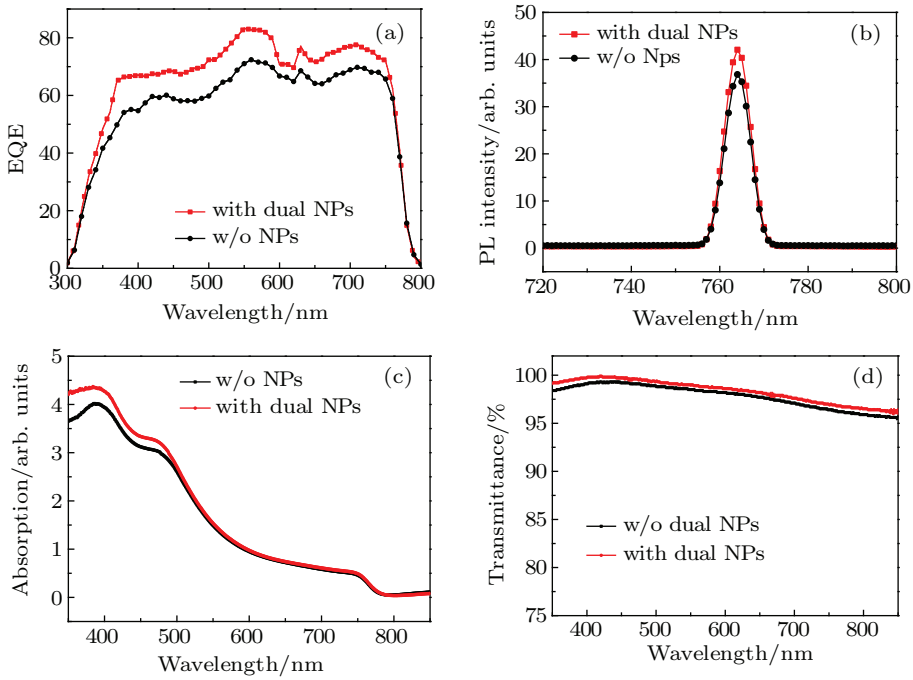


Fig. 5. (color online) (a) EQE spectra of the PSCs without and with dual NPs. (b) PL spectra of the PSCs without and with dual NPs recorded using excitation source wavelengths 380 nm. (c) UV–vis absorption spectra of ITO/PEDOT:PSS without and with dual NPs/$CH_3NH_3PbI_3$ films. (d) UV–vis absorption spectra of PEDOT:PSS without and with dual NPs films.

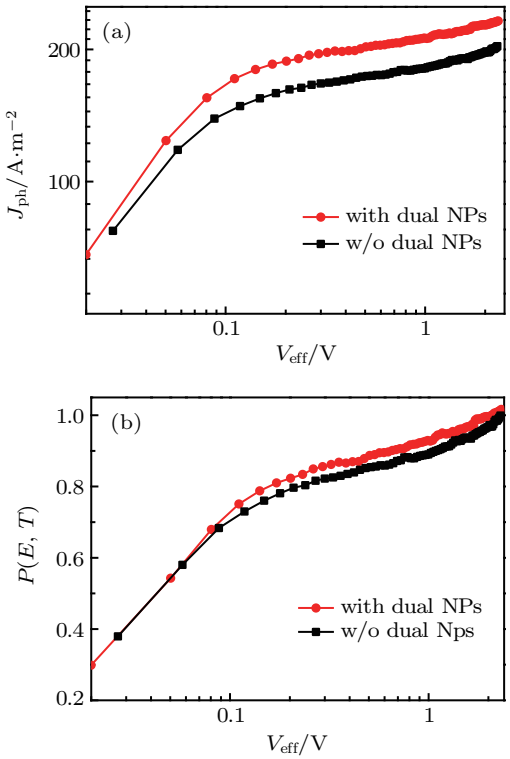


Fig. 6. (color online) (a) Photocurrent density plotted with respect to effective bias for the PSCs without and with dual NPs. (b) Charge carrier dissociation probability [$P(E,T)$] plotted with respect to effective bias for PSCs without and with dual NPs.

To further explore the effect of LSPR in PSCs, i.e., enhancement of the optical performance and improvement of the electrical performance, we denote the maximum charge carrier generation rate as G_{max} and charge carrier dissociation probabilities as $P(E,T)$ of our PSCs. The devices were biased sweeping from -1.5 to $+1.5$ V. Figure 6(a) reveals the effect of LSPR on photocurrent density (J_{ph}) versus effective voltage (V_{eff}) curve for our devices without and with NPs. Here, the J_{ph} is determined as $J_{ph} = J_L - J_D$, where J_L and J_D are the current density under illumination and in the dark, respectively. The V_{eff} is determined as $V_{eff} = V_0 - V_a$, where V_0 and V_a are the voltage at which $J_{ph} = 0$ and the applied bias voltage, respectively.[33] As shown in Fig. 6(a), we can get the value of the saturated current density which is only limited by total amount of absorbed incident photons.[34,35] We obtained the value of G_{max} by using the equation $J_{ph} = qG_{max}L$, where q and L are the electronic charge and the thickness of active layer (300 nm), respectively. The values of G_{max} for our devices without and with dual NPs are 4.23×10^{27} m^{-3}·s^{-1} (J_{sat} = 203.5 A·m^{-2}) and 4.75×10^{27} m^{-3}·s^{-1} (J_{sat} = 228.4 A·m^{-2}), respectively. An impressive enhancement of G_{max} occurred after incorporating dual NPs suggests that the light absorption increase in device with dual NPs.[34,35] We obtained the values of G_{max} by using the equation $J_{ph} = qG_{max}P(E,T)L$.[23] Figure 6(b) reveals that the value of $P(E,T)$ under the short-circuit conditions ($V_a = 0$ V) increases from 87.7% for the device without dual NPs to 91.4% for the device with NPs, indicating that excitation of the LSPR also contribute to the charge carriers dissociation. Thus, excitation of the LSPR promotes both the charge carrier generation and dissociation, improving the photocurrent of the PSCs.

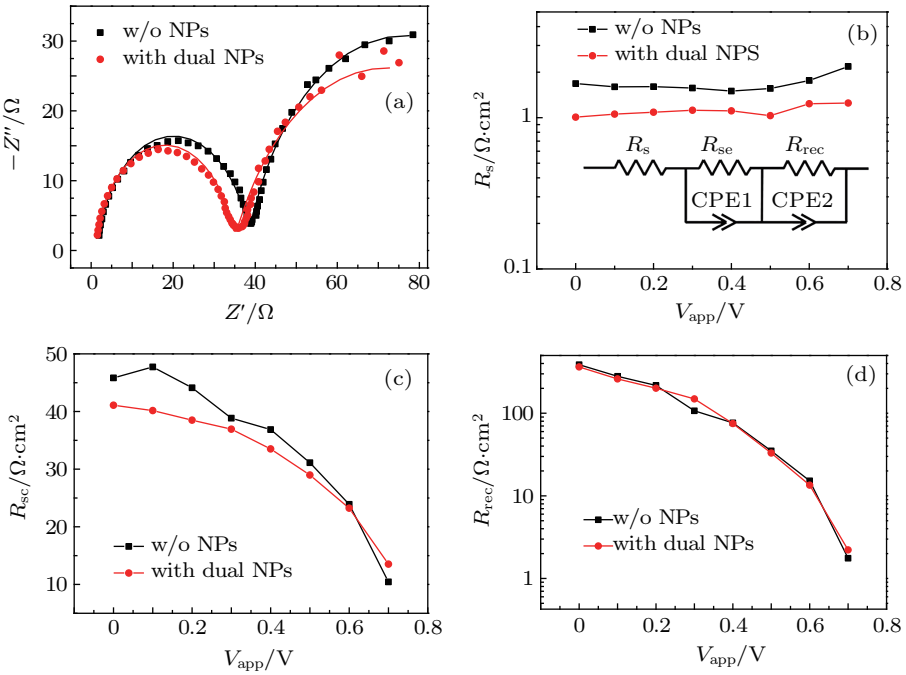


Fig. 7. (color online) (a) Nyquist plot of PSCs without and with dual NPs at DC bias of $V = 0.4$ V under 1 sun illumination. (b)–(d) Series resistance, resistance of the selective contacts, and recombination resistance of PSCs without and with dual NPs are presented, respectively. Equivalent model is included in the insert of panel (b).

To gain deeper insight into the influence of dual NPs on charge transfer in the devices, EIS spectra of PSCs without and with dual NPs were recorded under 1 sun AM 1.5G illumination with different bias voltage, as shown in Fig. A4 of Appendix A. Figure 7(a) shows the Nyquist plots (imaginary versus real part of the impedance) of devices without and with dual NPs at DC bias of $V = 0.4$ V. The impedance spectrum is basically formed by two arcs, one at medium frequency (low Z') and the other one at low frequency (high Z'), where the high frequency part is ascribed to the series resistance R_s, medium frequency part is attributed to selective contacts resistance R_{sc} and low frequency part is attributed to the recombination resistance R_{rec}.[36–38] Therefore, a simplified circuit model to fit the Nyquist plots in a homemade software is inserted in Fig. 7(b).[36–38] The constant phase elements (CPE) substitute ideal capacitors to improve the quality of fittings. Figures 7(b) and 7(c) present the series and selective contacts resistance for the PSCs without and with dual NPs under different bias voltages, respectively. It is found that the PSCs with dual NPs exhibit relative lower R_s and R_{sc} at given bias, indicating a more efficient charge transfer process at device with dual NPs. The variation trends of R_{rec} of device without and with dual NPs are shown in Fig. 7(d). We could observe that the PSCs without and with dual NPs present almost same R_{rec}, suggesting that the increase of charge recombination is avoided successfully when introducing dual NPs. These results suggest that introducing dual NPs into the HTL can enhance charge transport without increasing charge recombination, resulting in the increase of PCE.

4. Conclusions

In conclusion, we have developed an effective and simple strategy by embedding gold-silver dual NPs into the HTL of PSCs, which not only enhanced the optical performance. Due to the cooperative LSPR, average J_{sc} increases from 18.59 to 20.45 mA/cm^2, leading to increase of PCE from 10.4% to 11.6% (in average). The degree of light absorption, charge carrier generation, dissociation, and transportation in PSCs increase significantly as a result of LSPR-induced local field enhancement. We believe that the results reported here pave the way for the application of a variety of other nanoparticles in PSCs and fabrication of higher-efficiency PSCs.

Appendix A

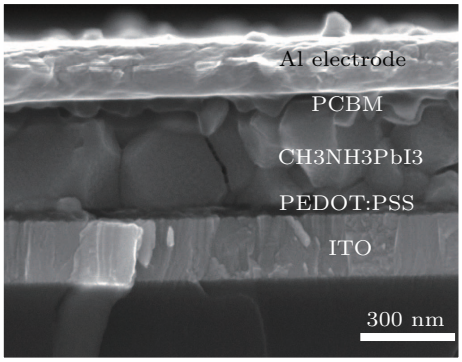


Fig. A1. Cross-section SEM image of perovskite device.

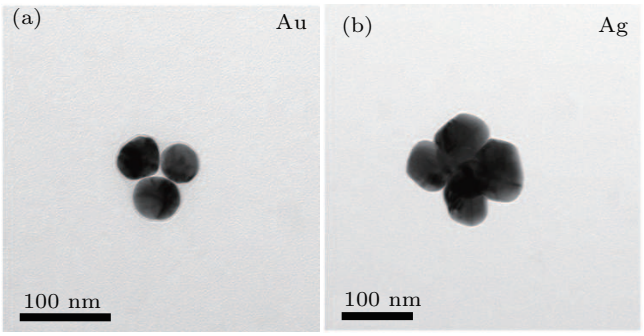


Fig. A2. (a) TEM images of Au. (b) TEM images of Ag.

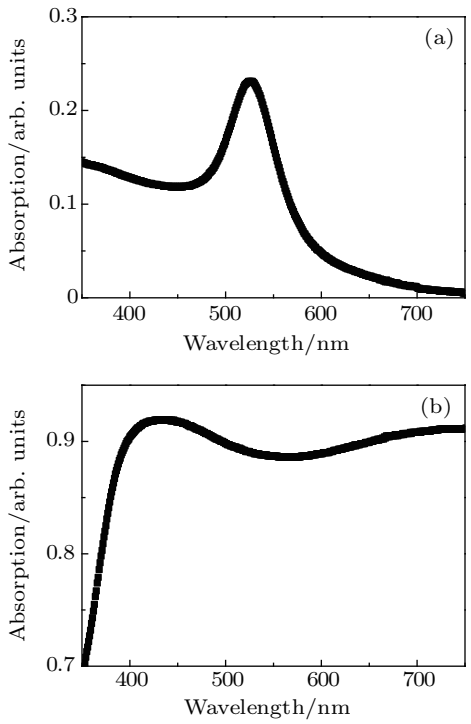


Fig. A3. Absorption spectrum of Au (a) and Ag (b) dispersed in deionized water.

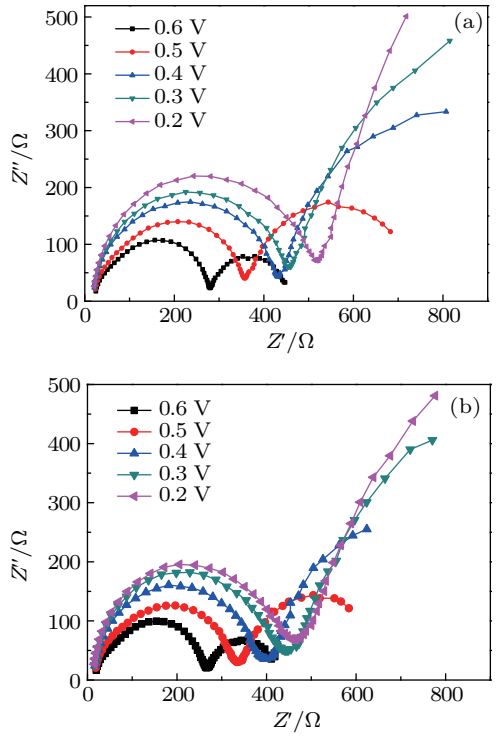


Fig. A4. (color online) Nyquist plot of devices without (a) and with (b) dual NPs at DC bias of 0.2, 0.3, 0.4, 0.5, and 0.6 V under 1 sun illumination.

References

[1] Xing G, Mathews N, Sun S, Lim S S, Lam Y M, Grätzel M, Mhaisalkar S and Sum T C 2013 *Science* **342** 344

[2] Wang J Z, Huang Q L, Xu X, Quan B G, Luo J H, Zhang Y, Ye J S, Li D M, Meng Q B and Yang G Z 2015 *Chin. Phys. B* **24** 329

[3] Dong Q, Fang Y, Shao Y, Mulligan P, Qiu J, Cao L and Huang J 2015 *Science* **347** 967

[4] Shao Y, Xiao Z, Bi C, Yuan Y and Huang J 2014 *Nat. Commun.* **5** 5784

[5] Bi C, Wang Q, Shao Y, Yuan Y, Xiao Z and Huang J 2015 *Nat. Commun.* **6** 7747

[6] Wu R, Yang B, Xiong J, Cao C, Huang Y, Wu F, Sun J, Zhou C, Huang H and Yang J 2015 *Renew. Sustain. Ener.* **7** 043105

[7] Zhou H, Chen Q, Li G, Luo S, Song T B, Duan H S, Hong Z, You J, Liu Y and Yang Y 2014 *Science* **345** 542

[8] Yin X, Yao Z, Luo Q, Dai X, Zhou Y, Zhang Y, Luo S, Li J and Wang N 2016 *ACS Appl. Mater. Inter.* **9** 2439

[9] Nie W, Tsai H, Asadpour R, Blancon J C, Neukirch A J, Gupta G, Crochet J J, Chhowalla M, Tretiak S and Alam M A 2015 *Science* **347** 522

[10] Burschka J, Pellet N, Moon S J, Humphry-Baker R, Gao P, Nazeeruddin M K and Grätzel M 2013 *Nature* **499** 316

[11] Liu M, Johnston M B and Snaith H J 2013 *Nature* **501** 395

[12] Docampo P, Ball J M, Darwich M, Eperon G E and Snaith H J 2013 *Nat. Commun.* **4** 2761

[13] Mei A, Li X, Liu L, Ku Z, Liu T, Rong Y, Xu M, Hu M, Chen J and Yang Y 2014 *Science* **345** 295

[14] Wang D L, Cui H J, Hou G J, Zhu Z G, Yan Q B and Su G 2016 *Sci. Rep.* **6** 18922

[15] Wu R, Yang B, Zhang C, Huang Y, Cui Y, Liu P, Zhou C, Hao Y, Gao Y and Yang J 2016 *J. Phys. Chem. C* **120** 6996

[16] Lee D S, Kim W, Cha B G, Kwon J, Kim S J, Kim M, Kim J, Wang D H and Park J H 2015 *ACS Appl. Mater. Inter.* **8** 449

[17] Hu Q, Wu H, Sun J, Yan D, Gao Y and Yang J 2016 *Nanoscale* **8** 5350

[18] Atwater H A and Polman A 2010 *Nat. Mater.* **9** 205

[19] Brown M D, Suteewong T, Kumar R S S, D'Innocenzo V, Petrozza A, Lee M M, Wiesner U and Snaith H J 2010 *Nano Lett.* **11** 438

[20] Leijtens T, Ding I K, Giovenzana T, Bloking J T, McGehee M D and Sellinger A 2012 *ACS Nano* **6** 1455

[21] Wang D H, Park K H, Seo J H, Seifter J, Jeon J H, Kim J K, Park J H, Park O O and Heeger A J 2011 *Adv. Ener. Mater.* **1** 766

[22] Wang C C, Choy W C, Duan C, Fung D D, Wei E, Xie F X, Huang F and Cao Y 2012 *J. Mater. Chem.* **22** 1206

[23] Heo M, Cho H, Jung J W, Jeong J R, Park S and Kim J Y 2011 *Adv. Mater.* **23** 5689

[24] Shalan A E, Oshikiri T, Sawayanagi H, Nakamura K, Ueno K, Sun Q, Wu H P, Diau W G and Misawa H 2016 *Nanoscale* **9** 1229

[25] Lu L, Luo Z, Xu T and Yu L 2012 *Nano Lett.* **13** 59

[26] Xiong J, Yang B, Wu R, Cao C, Huang Y, Liu C, Hu Z, Huang H, Gao Y and Yang J 2015 *Org. Electron.* **24** 106

[27] Wu R, Yang J, Xiong J, Liu P, Zhou C, Huang H, Gao Y and Yang B 2015 *Org. Electron.* **26** 265

[28] Xiao M, Huang F, Huang W, Dkhissi Y, Zhu Y, Etheridge J, Gray-Weale A, Bach U, Cheng Y B and Spiccia L 2014 *Angew. Chem.* **126** 10056

[29] Le Ru E, Etchegoin P, Grand J, Félidj N, Aubard J, Lévi G, Hohenau A and Krenn J 2008 *Curr. Appl. Phys.* **8** 467

[30] Lee J H, Park J H, Kim J S, Lee D Y and Cho K 2009 *Org. Electron.* **10** 416

[31] Mahmoud M A, Poncheri A J, Phillips R L and El-Sayed M A 2010 *J. Am. Chem. Soc.* **132** 2633

[32] Li X, Choy W C H, Lu H, Sha W E and Ho A H P 2013 *Funct. Mater.* **23** 2728

[33] Mihailetchi V, Wildeman J and Blom P 2005 *Phys. Rev. Lett.* **94** 126602

[34] Mihailetchi V, Koster L, Hummelen J and Blom P 2004 *Phys. Rev. Lett.* **93** 216601

[35] Shuttle C, Hamilton R, O'Regan B, Nelson J and Durrant J 2010 *P. Nat. A. Sci.* **107** 16448

[36] Kim H S, Mora-Sero I, Gonzalez-Pedro V, Fabregat-Santiago F, Juarez-Perez E J, Park N G and Bisquert J 2013 *Nat. Commun.* **4** 2242

[37] Liu Z, Shi T, Tang Z, Sun B and Liao G 2016 *Nanoscale* **8** 7017

[38] Gonzalez-Pedro V, Juarez-Perez E J, Arsyad W S, Barea E M, Fabregat-Santiago F, Mora-Sero I and Bisquert J 2014 *Nano Lett.* **14** 888